2nd International Conference on Engineering Optimization
September 6-9, 2010, Lisbon, Portugal

Structural Optimization of a Composite Plate subjected to a Small Mass Impact

Rafael Thiago Luiz Ferreira*, **Maurício Vicente Donadon**†, **José Antônio Hernandes**†

ITA - Instituto Tecnológico de Aeronáutica
*Divisão de Engenharia Mecânica-Aeronáutica
†Divisão de Engenharia Aeronáutica
12228-900 São José dos Campos - SP / Brasil
{rthiago, donadon, hernandes}@ita.br

Abstract
This paper presents the optimization of a composite plate subjected to a small mass impact under a mode II delamination constraint, considering impact response and delamination threshold load predicted by closed form solutions. These solutions are inexpensive from a computational point of view and have good agreement with experimental data. Therefore, this approach can be very interesting when working with optimization methods that require a large number of iterations to converge. In other hand, the closed form solutions have implicit limitations. An example is the plate and impactor masses ratio that must be within a defined range, otherwise the impact model do not apply. Consequently, the plate optimization problem must be well stated and constrained in order to provide results comprised in the closed form solutions validity. In this work, the optimization problem and strategy are stated and discussed, aiming to evaluate its application. The optimization method employed is the simulated annealing, together with appropriate optimization heuristics. Final optimization results are validated by finite element analysis with the capability of predicting damage in composites under impact.
Keywords: structural optimization, composite plates, small mass impact, delamination

1. Introduction

Impacts caused by runaway debris and hailstones in automobiles and aircraft are examples of low mass impacts (where the impactor mass is low in comparison with the mass of the structure being reached). In ref.[1], Olsson presents a model that describes the event of a small mass impacting a composite plate, based in the approximate analytical solution of a differential equation. This solution has shown good agreement with other numerical solutions (finite elements) and experimental data.
In composite structures, damage due to delamination is a main issue to consider in design. In ref.[2], Robinson and Davies proposed a criterion to predict the delamination onset load in composites subjected to transverse quasi-static loads. Furthermore, in ref.[3] by Olsson *et al.*, this criterion was reformulated to the specific case of small mass impacts, showing good agreement with experimental results.
Both the models to be used here, for predicting small mass impact response in composite plates [1] and delamination onset in such case [3], present solutions at a very low computational cost, specially when compared to finite elements (FE) analysis. Thus, both models seem to be very attractive for the use in structural optimization, and even more when the optimization method to be employed needs many evaluations of the function being minimized, as the case of the Simulated Annealing [4] (henceforth SA) here employed.
Nevertheless, both models have limitations, to be highlighted, that must be properly addressed during the optimization process. The aim of this paper is to evaluate the applicability of a optimization scheme based on them.

2. Impact Response Models

2.1. Small Mass Impact Model

When an impactor mass reaches a plate transversely at a certain velocity, the plate may assume different kind of responses. If the impactor mass is sufficiently low, the plate typical response is characterized by the propagation of flexural waves over its dominium, initiating in the impact point and reaching the plate boundaries. The impact force developed is out-of-phase with the displacements, whose magnitude is relatively small. This event is classified as the so-called small mass impact, which typically occurs if the impactor mass M is less than 1/4 of the mass M_p^* of the largest plate area affected by the flexural

waves, or:

$$M \leq M_p^*/4 \tag{1}$$

Following ref.[6], the area M_p^* is defined when the waves reach the plate boundaries and, according to Fig.1, this area is the area of an ellipse with semi-axis r_x, r_y, where:

$$r_x/r_y = (D_x/D_y)^{1/4} \qquad M_p^* = m\pi r_x r_y \tag{2}$$

In the Eq.(2), D_x and D_y are plate bending equivalent stiffnesses in the principal directions x, y and m is the plate mass per unit area. Ref.[5] presents a closed form solution for the Olsson's small mass impact model [1, 6], to be used here. This model considers that the impact of a small mass on a plate can be reduced to a mass-spring-dashpot system whose scheme and constants are shown in Fig.2. In this figure, M is the impactor mass, w_i is the impactor displacement, w_p is the plate deflection, k_α is the contact stiffness, q is an exponent, m is the plate mass per unit area and D^* is the effective plate bending stiffness. The definition of D^*, as well as the definition of an out-of-plane shear effective stiffness S^*, is given by the following:

$$D^* \approx \sqrt{D_{11}D_{22}(\eta+1)/2} \qquad \eta = (D_{12}+2D_{66})/\sqrt{D_{11}D_{22}} \tag{3}$$

$$S^* = \sqrt{K_{44}A_{44}K_{55}A_{55}} \tag{4}$$

In fact, the expression for D^* in Eq.(3) is a good approximation, specially for $\eta \simeq 1$ [5]. In the equations above, D_{11}, D_{22}, D_{12}, D_{66} are components of the plate bending stiffness matrix and A_{44}, A_{55} are the components of the out-of-plane shear stiffness matrix based on the Reissner-Mindlin laminated plate theory [7]. In Eq.(4), it may be assumed $K_{44} = K_{55} = 5/6$ as shear correction factors, as is usually done when working with this transverse shear plate theory.

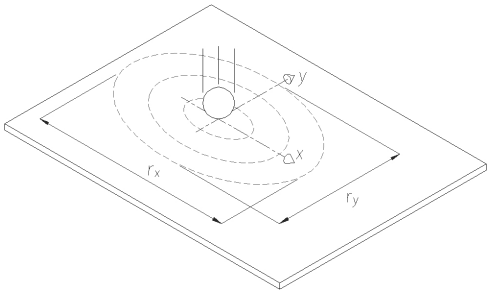

Figure 1: Ellipsoidal flexural waves caused by a small mass impact on a plate.

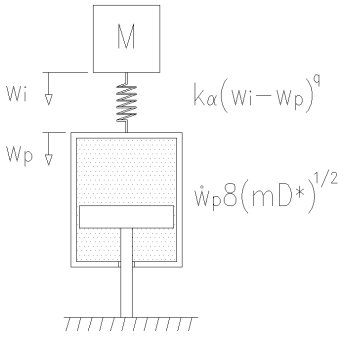

Figure 2: Schematic of the Olsson's small mass impact model.

The solution being followed is based on three asymptotic cases with deformation given purely by indentation, bending or shear. It predicts impact load peak and duration, as well as the deflection of a plate being reached by a mass M at a certain velocity V_0. Two dimensionless parameters are defined in the model: a bending parameter λ and a shear parameter β. When $\lambda = 0$, it means that the plate under impact has no bending mobility. When $\lambda = \infty$, the plate is fully mobile on bending. The same is valid for $\beta = 0$ and $\beta = \infty$, that means no mobility and full mobility on shear, respectively. Considering a mass M reaching the plate at a velocity V_0 and that the plate mass per unit area is $m = \rho h$ (plate density times plate thickness), these parameters are given by:

$$\lambda = M/\left(8T\sqrt{mD^*}\right) \qquad \beta = \sqrt{mD^*}/(TS^*) \tag{5}$$

In Eq.(5), T is a time constant defined by:

$$T = \left[M/\left(k_\alpha\sqrt{V_0}\right)\right]^{2/5} \tag{6}$$

In Eq.(6), k_α is the contact stiffness. This form of the time constant already considers a Hertzian load-indentation relationship given as follows:

$$F = k_\alpha \alpha^q \qquad \alpha = w_i - w_p \qquad q = 3/2 \tag{7}$$

In this equation, α is the indentation given by the difference between impactor displacement w_i and plate deflection w_p. The relation considers $q = 3/2$, what is true for monolithic laminates. The contact stiffness k_α takes into account the plate and impactor stiffnesses in transversal direction (Q_{zp} and Q_{zi} respectively), and is given by the following equations, considering R the impactor radius:

$$q = 3/2 \quad \Rightarrow \quad k_\alpha = (4/3)Q_\alpha\sqrt{R} \qquad\qquad Q_\alpha^{-1} = Q_{zp}^{-1} + Q_{zi}^{-1} \tag{8}$$

For a material with transverse isotropy, as may be presumed for monolithic laminates, the transverse stiffness Q_z can be taken [3, 8] as follows in Eqs.(9) and (10):

$$Q_z = \left[2\sqrt{G_{rz}/C_{rr}}\left(C_{rr}C_{zz} - C_{rz}^2\right)\right] \Big/ \left[\left(\sqrt{C_{rr}C_{zz}} + G_{zr}\right)^2 - (C_{rz} + G_{rz})^2\right]^{1/2} \tag{9}$$

$$C_{rr} = \frac{E_r(1 - \nu_{rz}\nu_{zr}\Omega)}{(1 + \nu_r)} \qquad C_{zz} = E_z(1 - \nu_r)\Omega \qquad C_{rz} = E_r\nu_{zr}\Omega \qquad \Omega = (1 - \nu_r - 2\nu_{rz}\nu_{zr})^{-1} \tag{10}$$

Isotropic materials are a special case where the Eq.(9) above simplifies to $Q_z = E/(1 - \nu^2)$. According to the solution being followed, an approximate solution for peak impact load F_{peak} is proposed as:

$$F_{peak}^{-1} \approx F_c^{-1} + F_b^{-1} + F_s^{-1} \tag{11}$$

In this equation, F_c is the contact load, the peak impact load when the plate is immobile in bending and shear ($\lambda = \beta = 0$). F_b is the bending load, the peak impact load when the plate is fully mobile in bending and immobile in shear ($\lambda = \infty$, $\beta = 0$). F_s is the shear force, the peak impact load when the plate is immobile in bending and is fully mobile in shear ($\lambda = 0$, $\beta = \infty$). The approximation in Eq.(11) is based in the estimation of the total plate mobility as a function of the plate mobilities in the three asymptotic cases described. The peak loads are given by:

$$q = 3/2 \quad \Rightarrow \quad F_c = k_\alpha^{2/5}\left[(5/4)MV_0^2\right]^{3/2} \qquad F_b = 8V_0\sqrt{mD^*} \qquad F_s = 2V_0\sqrt{\pi MS^*} \tag{12}$$

Additionally, the model roughly predicts the instant when peak load occurs as:

$$t_{peak} \leq 1.6T \tag{13}$$

Having the peak load and the time when it happens predicted, it is necessary to predict how is the shape of the impact load on time. A sinusoidal half-wave impulse could be a reasonable guess. In fact, ref.[6] shows that the impact load is sinusoidal if the bending parameter is $\lambda < 2$, and of course symmetrical in relation to t_{peak}, as shown in Fig.3(a). For $\lambda > 2$ the pulse starts to be non-symmetrical, as seen in Fig.3(b). So, a sinusoidal half-wave pulse is a good guess when $\lambda < 2$. Assuming the impact load as sinusoidal implies that its duration would be $2t_{peak}$. Moreover, it also implies that the impact is fully elastic and the peak plate deflection can be predicted [5] as:

$$w_p = (2MV_0) \Big/ \left(8\sqrt{mD^*}\right) \tag{14}$$

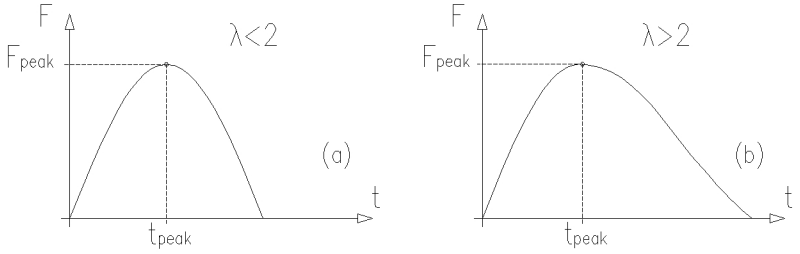

Figure 3: Impact force pulses, symmetrical for $\lambda < 2$ and non-symmetrical for $\lambda > 2$.

These expressions will be used in evaluating the plate response in the optimization scheme to be shown. However, for these predictions to be valid, it is necessary to ensure that $\lambda < 2$ and, first of all, that the impact is really a small mass impact case.

2.2. Delamination Threshold Load

Delamination is a main consideration in composites design. It occurs when, during an applied solicitation to a laminate, the interphase between two laminae fails and they are not bonded together anymore. As this fail occurs subsequently in a bigger delaminated area and/or in other pairs of sub-laminates, the laminated gradually looses its capabilities of transmitting stresses.

In ref.[2] it is deduced a criterion for the onset of mode II delamination considering a quasi-static loading in laminated composites. Mode II delamination is related to the occurrence of laminae debonding due to transverse shearing. In ref.[3], the criterion was adapted to the specific case of small mass impacts, by considering hypotheses on the dynamical behavior of the delamination initiation in such case. For the first delamination, it gives:

$$F_{d1}^{dyn} = 1.213\pi\sqrt{32 G_{IIc} D^* / 3} \tag{15}$$

In Eq.(15), D^* comes from Eq.(3) and G_{IIc} is the critical strain energy release rate in mode II, characteristic of the laminated material. This new criterion brought some improvement to the prediction of the mode II delamination onset in composite plates subjected to small mass impacts, in comparison to the predictions in ref.[2] and also with experimental data, as can be seen from ref.[3] itself.

Specifically, if the impact peak load reaches the delamination threshold load F_{d1}^{dyn}, the plate delaminates. This way, it is possible to think in characterizing a pulse, and therefore an impact event, that implies in delamination of the plate. When it is done, is possible to use the response of this impact event to constrain the plate response in the optimization process in order to avoid delamination in an optimized design. Taking Eq.(11), replacing F_{peak} by F_{d1}^{dyn} and considering a threshold impact velocity V_{d1} for delamination to occur, it is possible to write with the aid of Eqs.(12) and (15):

$$\left\{k_\alpha^{2/5}\left[(5/4)MV_{d1}^2\right]^{3/2}\right\}^{-1} + \left(8V_{d1}\sqrt{mD^*}\right)^{-1} + \left(2V_{d1}\sqrt{\pi M S^*}\right)^{-1} - \left(F_{d1}^{dyn}\right)^{-1} = 0 \tag{16}$$

By solving this transcendental equation in V_{d1}, it is possible to state the impact of a mass M that reaches the plate at the velocity V_{d1} that theoretically causes delamination in the structure. It is also possible to redefine the time constant T in Eq.(6) to such event, having the expression:

$$T_{d1} = \left[M / \left(k_\alpha\sqrt{V_{d1}}\right)\right]^{2/5} \tag{17}$$

With the time constant T_{d1} defined, it is possible to predict the instant when the peak load F_{d1}^{dyn} occurs, having as example Eq.(13):

$$t_{d1} \leq 1.6 T_{d1} \tag{18}$$

Ensuring $\lambda < 2$ as previously done, the impact load when delamination occurs is also a sinusoidal half-wave impulse of duration $2t_{d1}$. For this condition, it possible to predict a critical plate deflection w_{d1}, to be used in a delamination constraint throughout the optimization process. It has the same fashion as Eq.(14):

$$w_{d1} = (2MV_{d1}) / \left(8\sqrt{mD^*}\right) \tag{19}$$

3. Optimization Problem

Having defined properly the quantities that may define an optimization problem that considers a laminated plate subjected to a small mass impact, it is possible to state this problem as:

$$\begin{aligned}
\text{Minimize:} \quad & F(\{h_k\},\{\theta_k\},N_\ell) = p_1\frac{M_p}{M_p^0} + p_2\frac{w_p}{w_p^0} + p_3 P_{rep} \\
\text{Subject to:} \quad & g_w(\{h_k\},\{\theta_k\},N_\ell) = \frac{w_p}{w_{d1}} - 0.9 \leq 0 \\
& g_\lambda(\{h_k\},\{\theta_k\},N_\ell) = \frac{\lambda}{2} - 1 \leq 0 \\
& g_{sM}(\{h_k\},\{\theta_k\},N_\ell) = \frac{4M}{M_p^*} - 1 \leq 0 \\
\text{Where:} \quad & \{h_k\} = \{h_1 ... h_k ... h_{N_\ell}\} \quad \{\theta_k\} = \{\theta_1 ... \theta_k ... \theta_{N_\ell}\}
\end{aligned} \tag{20}$$

In Eq.(20), F is the objective function, a weighted sum of the plate mass M_p normalized by its initial value M_p^0, the plate peak deflection w_p normalized by its initial value w_p^0 and a penalty of repeated laminae P_{rep}. The weighting factors are p_1, p_2 and p_3. The plate peak deflection was added to the problem with a low weight p_2, to be stated, just to make F dependent on the plate stiffness. The penalty of repeated laminae P_{rep}, to be described, was considered in the problem aiming to avoid a large number of repeated laminae in the plate final design, which possibly leads to delamination.
The first problem constraint is g_w, that limits the plate peak displacement w_p in Eq.(14) to the plate critical displacement w_{d1} in Eq.(19), with a ten percent margin, trying to ensure that mode II delamination does not occur. The second constraint is g_λ and it limits the bending parameter λ to be less than 2, to ensure the validity of the solutions for displacements in Eqs.(14) and (19), as described in Sec.2.1. The last problem constraint is g_{sM} and ensures that a small mass impact really occurs, in the sense of respecting Eq.(1), which is necessary to the validity of both impact and delamination models here employed.
The problem design variables are $\{h_k\}$, $\{\theta_k\}$ and N_ℓ. The two first are, respectively, vectors of layer thicknesses and layer orientations of the laminated plate. N_ℓ is its number of layers.

4. Optimization Algorithm

In order to solve the optimization problem in Eq.(20), a FORTRAN code based in the SA method was developed, whose design evaluation is grounded in the impact and delamination models described. The code also includes proper heuristics for iterative design generation, as the SA requires. To incorporate the objective function F and the constraints g_w, g_λ and g_{sM} from Eq.(20), the technique of the interior penalty function [9] was used. Considering a pseudo-objective function Φ and penalty parameter r_p, it gives:

$$\Phi(\{h_k\},\{\theta_k\},N_\ell) = F + r_p\left\{max[0,g_w] + max[0,g_\lambda] + max[0,g_{sM}]\right\} \tag{21}$$

4.1. Simulated Annealing Method

The SA algorithm comes from the primal work by Metropolis *et al.* [10], which forms the basis for Monte Carlo statistical mechanics simulations of atomic and molecular systems. Its first employment in optimization is due to Kirkpatrick *et al.* [4]. The algorithm simulates, in an heuristic manner, the metallurgical process of annealing. In this process, a metallic material is heated up to a certain temperature and slowly cooled down to a predefined low temperature. This way, it is expected that the material molecules have time to arrange themselves in a minimum point (eventually global) of potential energy.
The use of the SA as an optimization method is grounded in analogies between the objective function of an optimization problem and the potential energy being minimized by the annealing process, and between the design variables of the problem and the molecules arrangement in the material under cooling. The basement of the method is the generation of new designs by perturbing a current design, according to numbers randomly generated, and whose acceptance or not is decided upon two criteria. If the new design decreases the current value of the objective function, it is promptly accepted. If it does not, the proposed new design may be accepted or not, based on a decision made by a probabilistic choice. This kind of move allows the algorithm to scape from local minimum points, instead of getting trapped on them, as commonly happens with directional search optimization methods [9].
Several authors have employed successfully the SA method in varied structural optimization scenarios, including laminated composite optimization [11, 12, 13, 14]. Specifically, the version of the algorithm used in this work is detailed in refs.[13, 14].

4.2. Heuristics for Design Generation

The SA method needs mechanisms for new design generation based on random changes of the current design, for evaluation and acceptance or not by the described criteria. With this purpose, a design generator was heuristically developed regarding laminate lay-up generation. It is divided in three schemes, described according to Tab.1. These design generation schemes are set as function of the current temperature range, such that as temperature cools off the proposed design changes become more limited. The temperature ranges are defined in Eq.(22), being based in the initial SA temperature T^0 and in the factors $1 > f_x^a > f_x^b > 0$:

$$T^a = f_x^a T^0 \qquad T^b = f_x^b T^0 \tag{22}$$

Table 1: Characteristics of the laminate lay-up generation in each of the temperature ranges.

First Temperature Range $T^0 > T^j \geq T^a$
- The number of layers N_ℓ are changed in $\pm t_x^{N1}\%$; - The orientation angles of $t_x^{C1}\%$ of the layers in $\{\theta_k\}$ are changed randomly; - The thicknesses of $t_x^{C1}\%$ of the layers in $\{h_k\}$ are changed randomly.
Second Temperature Range $T^a > T^j \geq T^b$
- The number of layers N_ℓ are changed in $\pm t_x^{N2}\%$, according to the probability p^{N2}; - The orientation angles of $t_x^{C2}\%$ of the layers in $\{\theta_k\}$ are changed in the neighborhood of the current values; - The thicknesses of $t_x^{C2}\%$ of the layers in $\{h_k\}$ are changed in the neighborhood of the current values.
Third Temperature Range $T^b > T^j > 0$
- The number of layers N_ℓ are not changed; - Or the orientation angles in $\{\theta_k\}$ or the thicknesses in $\{h_k\}$ of $t_x^{C3}\%$ of the layers are changed in the neighborhood of the current values.

It can be observed from Tab.1 that the modifications for each range become indeed more conservative as temperature decreases. For example, changes in the number of layers N_ℓ are done just in the first and second temperature ranges, and not in the third. Additionally, in the second range, these changes are done just according to a probability p^{N2}. These and all the other modifications can be controlled by parameters defined by percentages (like t_x^{N2}, p^{N2} and t_x^{C2} in the second temperature range), as well by changing the factors f_x^a and f_x^b in Eq.(22). Therefore, the generation scheme may be adapted to the SA needs by the tuning of the described percentage parameters. Moreover, there are also mechanisms for keeping the laminates always symmetric. See ref.[13] for all the details.
In all the ranges, the thicknesses and orientations in the vectors $\{h_k\}$ and $\{\theta_k\}$, respectively, have their values chosen in predefined lists of discrete values, say $\{h\}_{list}$ and $\{\theta\}_{list}$, and the variable of number of layers N_ℓ is kept inside predefined limits, ensuring that $N_\ell^{min} \leq N_\ell \leq N_\ell^{max}$.

4.3. Penalty of Repeated Laminae

A penalty of repeated laminae was included in the problem to avoid having groups of laminae with the same orientations stacked together, which favors delamination to occur. It is designated by P_{rep} in Eq.(20) and is based on checking all the $N_\ell - 1$ pairs of neighbor layers on a stacking sequence of a laminate. If the layers have the same orientation, a value of one is added up to the penalty. If not, the value added up to the penalty is zero, according to Eq.(23):

$$P_{rep} = \sum_{i=1}^{N_\ell - 1} c_i \qquad \text{where} \quad c_i = \begin{cases} 1 \text{ - if the neighbor layers have the same orientations} \\ 0 \text{ - if not} \end{cases} \tag{23}$$

5. Results

To evaluate the proposed optimization strategy, three laminates subject to small mass impacts were optimized. These cases are based on assuming as initial designs plates whose impact and delamination responses were well predicted by the impact and delamination models here discussed, as shown in refs.[5, 3]. Tab.2 shows the plates' details, all of them carbon-epoxy laminates.
In the SA optimizations, it was considered that the plates were square with dimensions $a = b = 127\ mm$. The quantities predicted by the models here employed are not dependent on boundary conditions. All the plates were submitted to small mass impacts whose impactor velocities V_0 and details are shown in Tab.3. In this table, it is also possible to see the SA tuning parameters, such as the initial temperature T_0 and the total number of iterations, as well as the percentages that give the design generation settings throughout the optimization (f_x^a, f_x^b, t_x^{N1}, t_x^{N2}, etc.). It is also specified the objective function weights and possible values to the design variables h_k, θ_k and the limits to the design variable N_ℓ, among other quantities necessary to fully define the optimization process.

Table 2: Details of the laminated materials of the plates in their initial designs.

Material	E_{11}	E_{22} E_{33}	G_{12} G_{13}	G_{23} (GPa)	v_{12} v_{13}	v_{23}	Density (kg/m^3)	G_{IIc} (J/m^2)	Initial Stacking Sequence
HTA/6376C	137	10.4	5.2	3.5	0.3	0.51	1620	600	$\{\theta_k\} = [(0/\pm 45/90)_s/(90/\mp 45/0)_s]_3$ $h_k = 0.130\ mm$
T300/5208	132	10.8	5.6	4.4	0.24	0.5	1600	300	$\{\theta_k\} = [0/\pm 45/90]_{6s}$ $h_k = 0.127\ mm$
XAS/914C	145	9.5	5.6	3.6	0.31	0.5	1600	416	$\{\theta_k\} = [0_2/\pm 45]_{2s}$ $h_k = 0.125\ mm$

Table 3: Optimization data and results for the cases considered.

Optimization Cases	HTA/6376C	T300/5208	XAS/914C
Impactor Data			
$M\ (g)$, $R\ (mm)$, $V_0\ (m/s)$	10.2, 11, 23	3, 6.4, 27	0.9, 3, 24
Material	Aluminium $E = 71\ GPa$, $\nu = 0.3$	Aluminium $E = 71\ GPa$, $\nu = 0.3$	Steel $E = 206\ GPa$, $\nu = 0.3$
Optimization Settings			
T^0	10		
Total SA Iterations	1000 (40 temperature loops with 25 iterations each)		
f_x^a, f_x^b	0.7, 0.2	0.8, 0.2	0.7, 0.2
t_x^{N1}, t_x^{C1}	0.1, 0.1	0.15, 0.15	0.1, 0.1
t_x^{N2}, t_x^{C2}, p^{N2}	0.07, 0.07, 0.7	0.07, 0.07, 0.7	0.07, 0.07, 0.7
t_x^{C3}	0.05	0.05	0.05
p_1, p_2, p_3, r_p	1, 0.05, 10, 100	1, 0.05, 10, 100	1, 0.05, 10, 100
$\{h\}_{list}\ (mm)$	$\{0.100, 0.130, 0.160\}$	$\{0.097, 0.127, 0.157\}$	$\{0.095, 0.125, 0.155\}$
$\{\theta\}_{list}\ (^\circ)$	$\{0, \pm 45, 90\}$	$\{0, \pm 45, 90\}$	$\{0, \pm 45, 90\}$
N_ℓ^{min}, N_ℓ^{max}	6, 50	6, 50	20, 6
Optimization Results			
M_p [Initial/Final] ([I/F]) (g)	163.04 / 102.42 (-37%)	157.31 / 128.23 (-18%)	51.61 / 43.74 (-15%)
w_p [I/F] (mm)	0.518 / 1.314	0.192 / 0.290	0.514 / 0.639
w_{d1} [I/F] (mm)	0.697 / 1.463	0.250 / 0.322	0.683 / 0.835
λ [I/F]	0.785 / 1.991	0.377 / 0.567	1.609 / 1.993
g_w [I/F]	-0.156 / -0.002	-0.129 / -0.0004	-0.148 / -0.151
g_λ [I/F]	-0.607 / -0.004	-0.810 / -0.716	-0.195 / -0.003
g_{sM} [I/F]	-0.920 / -0.872	-0.974 / -0.970	-0.967 / 0.973
P_{rep} [I/F]	7 / 0	1 / 0	5 / 0
Φ [I/F]	71.050 / 0.755	11.050 / 0.890	51.05 / 0.909

Table 4: Stacking sequence details of the final optimized designs.

Material	Final Optimized Stacking Sequence
HTA/6376C	$\{\theta_k\} = [90/-45/0/45/0/(-45/45)_2/0/90/0/45/90/\overline{0}]_s$
	$\{h_k\} = [(160)_2/130/(100)_2/130/100/160/(130)_2/(160)_2/(130)_2/\overline{160}]_s\ \times 10^{-3} mm$
T300/5208	$\{\theta_k\} = [0/-45/90/-45/45/-45/0/-45/90/45/0/45/(90/0)_2/90/-45/\overline{0}]_s$
	$\{h_k\} = [97/127/(157)_2/97/(127)_4/157/(127)_2/(157)_2/97/157/127/(\overline{157})_2]_s\ \times 10^{-3} mm$
XAS/914C	$\{\theta_k\} = [45/90/0/45/0/-45/0/\overline{45}]_s$
	$\{h_k\} = [(95)_2/(125)_2/95/155/95/\overline{125}]_s\ \times 10^{-3} mm$

The optimization results for the three cases considered are depicted in Tab.3 as well, in its last section. In these results, it is noticeable that a mass reduction was obtained for all the cases. The constraints in the initial designs, all feasible, remained feasible during the optimization processes, with some of them becoming active, like the delamination constraints g_w for the HTA/6376C and T300/5208 cases. The constraints regarding the validity of the impact and delamination models here employed, g_λ and g_{sM}, did not interfere to the optimization process, except in the XAS/914C case. In this case, the constraint g_λ became active before the displacement constraint g_w, indicating that the plate mass could not be further

reduced without violating $\lambda < 2$, as required to the model applicability. Tab.4 shows the final stacking sequences obtained for the three laminates in the optimization cases discussed. From this results, it is possible to notice that the penalty of repeated laminae P_{rep} was effective in removing pairs of layers with the same orientations of these final designs.
It is worth highlighting that the full SA runs, with 1000 iterations each, took less than one minute each to be completed in a regular PC. If the impact and delamination responses were predicted by finite elements, for example, the runs would certainly take several hours.

6. Model Validation

The optimized laminates obtained for the three impact cases presented in the previous section were validated by finite element analyses. The finite element model consists of two sub-laminates with half of the total plate thickness each, modeled with thick shell elements. The sub-laminates were connected with a three-dimensional interface element placed at the midplane of the laminate. The connection between the interface layer and the two sub-laminates was performed using the Tie option available in ABAQUS FE code. The shell thickness effect was taken into account in the Tie option in order to ensure the kinematics compatibility between shell and solid elements. The interface layer has a thickness of 0.01 mm. The impactor was modeled using discrete rigid elements available in ABAQUS FE code. A penalty based formulation contact logic was used to model the contact between the plate and the impactor. The FE mesh used in the simulations is shown in Fig.4. The three dimensional interface element was implemented as an user-defined material model within a single integration point solid element available in ABAQUS/Explicit. The interfacial material behavior is defined in terms of tractions and relative displacements between the upper and lower surfaces defining the interface. The relative displacement vector is composed of the resultant normal and sliding components defined by the relative movement between upper and lower surfaces of the contact element (see Fig.5(a)).

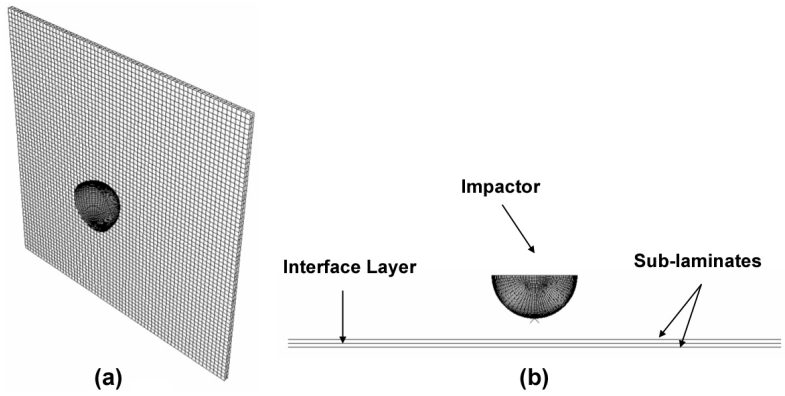

Figure 4: Details of the finite element model for optimization validation.

The criteria for damage initiation and damage progression are respectively given by Eqs.(24) and (25). The constitutive law for a three dimensional stress case is shown in Fig.5(b). G_i is the strain energy released rate defined by Eq.(26). K_i is the interfacial stiffness in the direction $i = I, II, III$, for mode I, II and III, respectively. d is the damage parameter defined in Eq.(27). N, S_{II} and S_{III} are the inter-laminar strengths associated with mode I, II and III, respectively. μ is the power law coefficient. The mixed-mode delamination damage onset displacement vector is given in Eq.(28), and the final resultant displacement associated with the fully debonded interfacial behavior, is given in Eq.(29). α_i and β_i are defined in Fig.5(c), and they are the angles that define the orientation of the relative displacement vector. Details about the formulation are given in ref.[15]. The material model parameters used in the simulations were $N = 60\ MPa$, $S_{II} = S_{III} = 100\ MPa$, $G_{I_c} = 300\ J/m^2$, $G_{IIIc} = G_{IIc}$ and $\mu = 1$, in all the cases.

$$\left(\frac{\max(\sigma_I, 0)}{N}\right)^2 + \left(\frac{\sigma_{II}}{S_{II}}\right)^2 + \left(\frac{\sigma_{III}}{S_{III}}\right)^2 = 1 \tag{24}$$

$$\left(\frac{G_I}{G_{Ic}}\right)^{\mu} + \left(\frac{G_{II}}{G_{IIc}}\right)^{\mu} + \left(\frac{G_{III}}{G_{IIIc}}\right)^{\mu} = 1 \tag{25}$$

$$G_i = \int_0^{\delta_i^f} \sigma_i d\delta_i \quad \rightarrow \quad \sigma_i = K_i(1-d)\delta_i \tag{26}$$

$$d = 1 - \frac{\bar{\delta}_0}{\bar{\delta}}\left[1 + \left(\frac{\bar{\delta}-\bar{\delta}_0}{\bar{\delta}_f-\bar{\delta}_0}\right)\left(2\left(\frac{\bar{\delta}-\bar{\delta}_0}{\bar{\delta}_f-\bar{\delta}_0}\right)-3\right)\right] \quad \text{with} \quad \bar{\delta} = \sqrt{u^2+v^2+w^2} \tag{27}$$

$$\bar{\delta}_0 = \left[\left(\frac{K_I \cos\beta_i}{N}\right)^2 + \left(\frac{K_{II}\sin\beta_i\cos\alpha_i}{S_{II}}\right)^2 + \left(\frac{K_{III}\sin\beta_i\sin\alpha_i}{S_{III}}\right)^2\right]^{-1/2} \tag{28}$$

$$\bar{\delta}_f = \frac{2}{\bar{\delta}_0}\left[\left(\frac{K_I \cos\beta_i}{G_{Ic}}\right)^\mu + \left(\frac{K_{II}\sin\beta_i\cos\alpha_i}{G_{IIc}}\right)^\mu + \left(\frac{K_{III}\sin\beta_i\sin\alpha_i}{G_{IIIc}}\right)^\mu\right]^{-1/\mu} \tag{29}$$

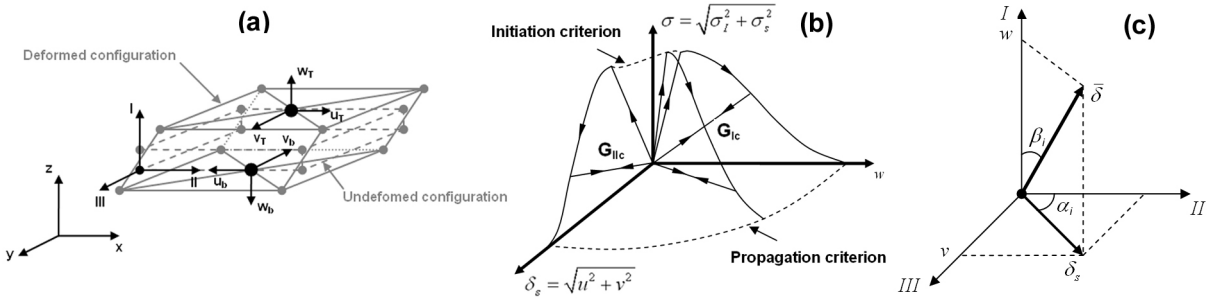

Figure 5: Interface element details.

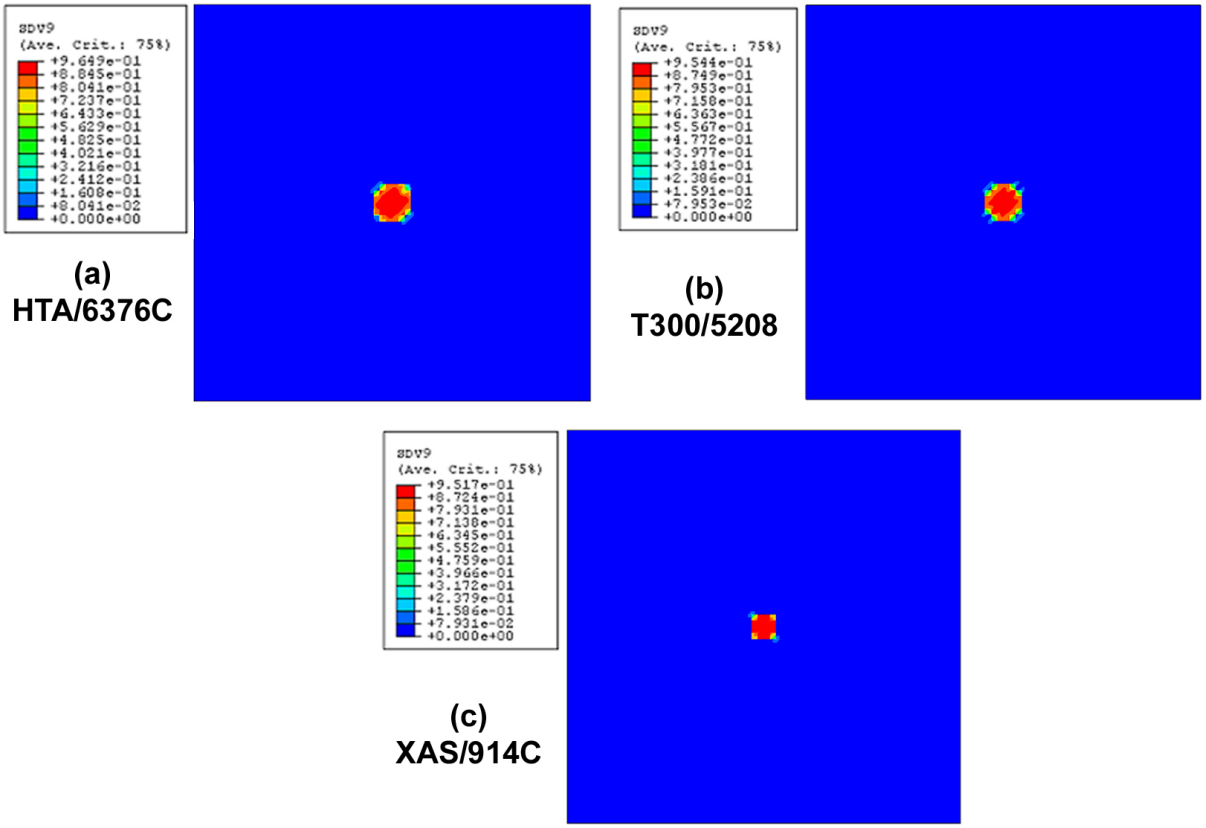

Figure 6: Predicted delamination patterns validating the optimization cases here presented.

Fig.6 shows the damage patterns for the three cases studied in this work. The numerical predictions indicated that the damage parameter d is lower than 1 for all cases. It is worth noticing that $d = 1$ means that there is fully debonding between upper and lower sub-laminates. Thus, no debonding between upper and lower sub-laminates was observed for the three proposed optimized laminates.

7. Conclusions

The validity of an impact optimization scheme based on impact and delamination analytical models was demonstrated. The limitations of the models were not a serious drawback, as the optimization results indicated.

The results obtained were successfully validated by finite element impact models with the capability of predicting delamination, showing that is possible to save computational time by using such methodology.

References

[**1**] R. Olsson, Impact response of orthotropic composite plates predicted from a one-parameter differential equation, *AIAA Journal*, 30 (6), 1587-1595, 1992.

[**2**] P. Robinson and G.A.O. Davies, Impactor mass and specimen geometry effects in low velocity impact of laminated composites, *International Journal of Impact Engineering*, 12, 189-207, 1992.

[**3**] R. Olsson, M.V. Donadon and B.G. Falzon, Delamination threshold load for dynamic impact on plates, *International Journal of Solids and Structures*, 43, 3124-3141, 2006.

[**4**] S. Kirkpatrick, C.D. Gelatt and M.P. Veochi, Optimization by simulated annealing, *Science*, 220 (4958), 671-680, 1983.

[**5**] R. Olsson, Closed form prediction of peak load and delamination onset under small mass impact, *Composite Structures*, 59, 341-349, 2003.

[**6**] R. Olsson, Engineering method for prediction of impact response and damage in sandwich panels, *Journal of Sandwich Structures and Materials*, 4, 3-29, 2002.

[**7**] J.N. Reddy, *Mechanics of Laminated Composite Plates: Theory and Analysis*, CRC Press, Boca Raton, 1997.

[**8**] L.B. Greszczuk, *Damage in composite materials due to low velocity impact*, In: J.A. Zukas et al., Impact Dymanics, John Wiley and Sons, New York, 1982.

[**9**] G.N. Vanderplaats, *Numerical optimization techniques for engineering design*, McGraw-Hill, New York, 1984.

[**10**] N. Metropolis, A.W. Rosenbluth, M.N Rosenbluth, A. Teller and E. Teller, Equations of state calculations by fast computing machines, *Journal of Chemical Physics*, 21 (6), 1087-1092, 1953.

[**11**] O. Erdal and F.O. Sonmez, Optimum design of composite laminates for maximum buckling load capacity using simulated annealing, *Composite Structures*, 71, 45-52, 2005.

[**12**] S. Deng, P.F. Pai, C.C Lai and P.S. Wu, A solution to the stacking sequence of a composite laminate plate with constant thickness using simulated annealing algorithms, *The International Journal of Advanced Manufacturing Technology*, 26, 499-504, 2005.

[**13**] R.T.L. Ferreira, *Otimização de placas laminadas sujeitas a cargas-pulso.* Master's thesis, ITA - Instituto Tecnólogico de Aeronáutica, São José dos Campos - SP, Brasil, 2008.

[**14**] R.T.L. Ferreira, J.A. Hernandes, E. Lucena Neto and P.I.B. de Queirós, Optimization of laminated plates subjected to impulse loads, *XXIX Iberian Latin American Congress on Computational Methods in Engineering*, ABMEC, Maceió - AL, Brazil, 2008.

[**15**] M.V. Donadon and S.F.M. Almeida, A contact-logic for mixed-mode modelling in composite laminates, To be submitted to *International Journal of Aerospace Engineering*, 2009.